EIT Image Reconstruction by Simultaneous Perturbation Method

Ho-Chan Kim*, Chang-Jin Boo*, and Yoon-Joon Lee**

* Department of Electrical Engineering, Cheju National University, Jeju, Korea
(Tel : +82-64-754-3676; E-mail: hckim@cheju.ac.kr , boo1004@cheju.ac.kr)
** Department of Nuclear and Energy Engineering, Cheju National University,Jeju, Korea
(Tel : +82-64-754-3641; E-mail:leeyj@cheju.ac.kr)

Abstract: In electrical impedance tomography (EIT), various image reconstruction algorithms have been used in order to compute the internal resistivity distribution of the unknown object with its electric potential data at the boundary. Mathematically the EIT image reconstruction algorithm is a nonlinear ill-posed inverse problem. This paper presents a simultaneous perturbation method as an image reconstruction algorithm for the solution of the static EIT inverse problem. Computer simulations with the 32 channels synthetic data show that the spatial resolution of reconstructed images by the proposed scheme is improved as compared to that of the mNR algorithm at the expense of increased computational burden.

Keywords: Electrical impedance tomography, Simultaneous perturbation method, Inverse problem, Finite element method,

1. INTRODUCTION

Electrical impedance tomography (EIT) plays an important role as a new monitoring tool for engineering applications such as biomedical imaging and process tomography, due to its relatively cheap electronic hardware requirements and nonintrusive measurement property [1-3]. In EIT, different current patterns are injected to the unknown object through electrodes and the corresponding voltages are measured on its boundary surface. The physical relationship between inner resistivity (or conductivity) and boundary surface voltage is governed by the nonlinear Laplace equation with appropriate boundary conditions, so that it is impossible to obtain the closed-form solution for the resistivity distribution. Hence, the internal resistivity distribution of the unknown object is computed using the boundary voltage data based on various reconstruction algorithms.

Yorkey *et al.* [4] developed a modified Newton-Raphson (mNR) algorithm for a static EIT image reconstruction and compared it with other existing algorithms such as backprojection, perturbation and double constraints methods. They concluded that the mNR reveals relatively good performance in terms of convergence rate and residual error compared to those of the other methods. However, in real situations, the mNR method is often failed to obtain satisfactory images from physical data due to large modeling error, poor signal to noise ratios (SNRs) and ill-conditioned (ill-posed) characteristics. That is, the ratio between the maximum and minimum eigenvalues of the information matrix (or Hessian matrix) is very large. In particular, the ill-conditioning of the information matrix results in an inaccurate matrix inverse so that the resistivity update process is very sensitive to the modeling and measurement errors. So, there is considerable interest in techniques for optimization that rely on measurements of the cost function only, not on measurements (or direct calculations) of the gradient (or higher order derivatives) of the cost function.

One of the techniques using only cost function measurements that has attracted considerable recent attention for difficult multivariate problems is the simultaneous perturbation stochastic approximation (SPSA) method introduced in Spall [5] and more fully analyzed in Spall [6]. SPSA is based on a highly efficient and easily implemented "simultaneous perturbation" approximation to the gradient: this gradient approximation uses only two cost function measurements independent of the number of parameters (say, p) being optimized. This contrasts, for example, with the standard (two-sided) finite-difference stochastic approximation (FDSA) [7], which uses $2p$ function measurements to approximate the gradient.

The major difficulties in impedance imaging are in the nonlinearity of the problem itself and the poor sensitivity of the boundary voltages to the resistivity of the flow domain deep inside. Several researchers suggested various element or mesh grouping methods where they force all meshes belonging to certain groups to have the same resistivity values [8,9].

In this paper, we will discuss the image reconstruction in EIT based on combining SPSA and mNR algorithms. We have broken the procedure for obtaining the internal resistivity distribution into two steps. In the first step, each mesh is classified into three mesh groups: target, background, and temporary groups. After a few iteration of mNR algorithm, an absolute values of meshes can not be determined but some useful informations on the target images be given. So, we use the mNR algorithm to determine the resistivity of meshes and rearrange the resisitivity values of meshes by sorting them in ascending order. Then the boundary location between regions can be roughly decided and mesh be determined to the target, background, or undetermined temporary group. In the second step, the values of these resistivities are determined using SPSA algorithm. This two-step approach allows us to better constrain the inverse problem and subsequently achieve a higher spatial resolution

2. IMAGE RECONSTRUCTION USING SPSA ALGORITHM IN EIT

The numerical algorithm used to convert the electrical measurements at the boundary to a resistivity distribution is described here. The algorithm consists of iteratively solving the forward problem and updating the resistivity distribution as dictated by the formulation of the inverse problem. The forward problem of EIT calculates boundary potentials with the given electrical resistivity distribution, and the inverse problem of EIT takes potential measurements at the boundary to update the resistivity distribution.

2.1 The forward problem

The first When electrical currents $I_l (l = 1, \cdots, L)$ are injected into the object $\Omega \in R^2$ through electrodes

$e_l (l = 1, \cdots, L)$ attached on the boundary $\partial\Omega$ and the resistivity distribution $\rho(x, y)$ is known over Ω, the corresponding induced electrical potential $u(x, y)$ can be determined uniquely from the nonlinear Laplace equation which can be derived from the Maxwell equation, Ohm's law, and the Neumann type boundary condition. The complete electrode model takes into account both the shunting effect of the electrode and the contact impedances between the electrodes and the object. The equations of complete electrode model are

$$\nabla \cdot (\rho^{-1} \nabla u) = 0 \text{ in } \Omega \tag{1}$$

$$\int_{e_l} \rho^{-1} \frac{\partial u}{\partial n} dS = I_l, \; l = 1, \cdots, L$$

$$u + z_l \rho^{-1} \frac{\partial u}{\partial n} = U_l \text{ on } e_l, \; l = 1, \cdots, L \tag{2}$$

$$\rho^{-1} \frac{\partial u}{\partial n} = 0 \text{ on } \partial\Omega \setminus \bigcup_{l=1}^{L} e_l$$

where z_l is effective contact impedance between the l th electrode and the object, U_l is the measured potential at the l th electrode and n is outward unit normal. In addition, we have the following two conditions for the injected currents and measured voltages by taking into account the conservation of electrical charge and appropriate selection of ground electrode, respectively.

$$\sum_{l=1}^{L} I_l = 0, \tag{3}$$

$$\sum_{l=1}^{L} U_l = 0. \tag{4}$$

The computation of the potential $u(x, y)$ for the given resistivity distribution $\rho(x, y)$ and boundary condition I_l is called the forward problem. The numerical solution for the forward problem can be obtained using the finite element method (FEM). In the FEM, the object area is discretized into small elements having a node at each corner. It is assumed that the resistivity distribution is constant within an element. The potential at each node is calculated by discretizing (1) into $Yu = c$, where u is the vector of boundary potential, c the vector of injected current patterns and the matrix Y is a functions of the unknown resistivities.

2.2 The inverse problem

The inverse problem, also known as the image reconstruction, consists in reconstructing the resistivity distribution $\rho(x, y)$ from potential differences measured on the boundary of the object. Ideally, knowing the potential on the whole boundary makes the correspondence between the resistivity distribution and the potential biunique. The relatively simple situation depicted so far does not hold exactly in the real world. The methods used for solving the EIT problem search for an approximate solution, i.e., for a resistivity distribution minimizing some sort of residual involving the measured and calculated potential values. From a mathematical point of view, the EIT inverse problem consists in finding the coordinates of a point in a M-dimensional hyperspace, where M is the number of discrete elements whose union constitutes the tomographic section under consideration. In the past, several EIT image reconstruction algorithms for the current injection method have been developed by various authors. A review of these methods is given in [10]. To reconstruct the resistivity distribution inside the object, we have to solve the nonlinear ill-posed inverse problem. Regularization techniques are needed to weaken the ill-posedness and to obtain stable solutions.

Generalized Tikhonov regularized version of the EIT inverse problem can be written in the form [3]

$$\Psi(\rho) = \min_{\rho} \{ \| U - V(\rho) \|^2 + \lambda \| R\rho \|^2 \} \tag{5}$$

where $\rho \in R^N$ is the resistivity distribution. $V(\rho) \in R^{LK}$ is the vector of voltages obtained from the model with known ρ, $U \in R^{LK}$ are the measured voltages and R and λ are the regularization matrix and the regularization parameter, respectively. L and K are the numbers of electrodes on the surface and injected current patterns, respectively. There are many approaches in the literature [11-14] to determine R and α, but the usual choice is to fix $R = I_M$ with the identity matrix and to adjust λ empirically.

Minimizing the objective function $\Psi(\rho)$ gives an equation for the update of the resistivity vector

$$\begin{aligned} \rho_{k+1} &= \rho_k + \Delta\rho_{k+1} \\ \Delta\rho_{k+1} &= (H_k + \lambda I)^{-1} \{ J_k^T (U - V(\rho_k)) - \lambda \rho_k \} \end{aligned} \tag{6}$$

where the partial derivative of Ψ with respect to ρ has been approximately by a Taylor series expansion around ρ_k. The Jacobian J_k is a matrix composed of the derivative of the vector of predicted potentials with respect to the unknown resistivities. The Jacobian is derived from the finite element formulation given by $J_k = \left. \frac{\partial \Psi}{\partial \rho} \right|_{\rho_k}$. The Hessian H_k is the second derivative of the predicted potentials with respect to the resistivity and is approximated as the square of the Jacobian for computational efficiency. Since the objective function $\Psi(\rho)$ is multimodal (i.e., it presents several local minima), the inversion procedure does not always converge to the true solution. The reconstruction algorithms are likely to be trapped in a local minimum and sometimes the best solution of a static EIT problem is rather unsatisfactory.

This study attempts to apply SPSA to EIT image reconstruction. The characteristics of SPSA algorithms appears to be of value in EIT reconstruction; no evaluation of

function derivatives is needed. The preceding considerations suggest the viability of employing SPSA's for the solution of the EIT problem, according to the procedure described in the following section.

2.3 The basic SPSA algorithm

The goal is to minimize a cost function $E(\theta)$, where the cost function is a scalar-valued "performance measure" and θ is a continuous-valued P-dimensional vector of parameters to be adjusted. The SPSA algorithm works by iterating from an initial guess of the optimal, where the iteration process depends on the above-mentioned highly efficient "simultaneous perturbation" approximation to the gradient $g(\theta) \equiv \partial E(\theta)/\partial\theta$.

Assume that measurements of the cost function are available at any value of θ:

$$y(\theta) = E(\theta) + noise$$

For example, in a Monte Carlo simulation-based optimization context, $E(\theta)$ may represent the mean response with input parameters θ, and $y(\theta)$ may represent the outcome of one simulation experiment at θ. In some problems, exact cost function measurements will be available. This corresponds to the $noise = 0$ setting (and in the simulation example, would correspond to a deterministic non-Monte Carlo-simulation). Note that no direct measurements (with or without noise) of the gradient are assumed available. This measurement formulation is identical to that of the FDSA algorithm and most implementations of genetic optimization algorithms and simulated annealing. It differs from Newton-Raphson search, and maximum likelihood scoring, all of which require direct measurement or calculation of $g(\theta)$.

It is assumed that $E(\theta)$ is a differentiable function of θ and that the minimum point θ^* corresponds to a zero point of the gradient, i.e.,

$$g(\theta^*) = \left.\frac{\partial E(\theta)}{\partial\theta}\right|_{\theta=\theta^*} = 0 \tag{7}$$

In cases where more than one point satisfies (7), then the algorithm may only converge to a local minimum (as a consequence of the basic recursive form of the algorithm there is generally not a risk of converging to a maximum or saddlepoint of $E(\theta)$, i.e., to nonminimum points where $g(\theta)$ may equal zero). The modifications of basic SPSA algorithm allow it to search for the global solution among multiple local solutions. Note also that (7) is generally associated with unconstrained optimization; however, through the application of penalty function and/or projection methods, it is possible to use (7) in a constrained problem (i.e., one where the θ values are not allowed to obtain certain values, usually as specified through equality and inequality constraints on the values of θ or $E(\theta)$.

2.4 The SPSA algorithm approach to EIT

In some applications like visualization of two-component systems, we may assume that there are only two different representative resistivity values; one resistivity value for the background and the other for the target. Here, the target need not be a single segment. It may be composed of multiple segments of the same resistivity value [15].

In this paper, we will discuss the image reconstruction in EIT using two-step approach. We have broken the procedure for obtaining the internal resisitivity distribution into two steps. In the first step, we adopted a mNR method as a basic image reconstruction algorithm. After a few initial mNR iterations performed without any grouping, we classify each mesh into one of three mesh groups: BackGroup (or TargetGroup) is the mesh group with the resistivity value of the background (or target). TempGroup is the group of meshes neither in BackGroup nor in TargetGroup. All meshes in BackGroup and in TargetGroup are forced to have the same but unknown resistivity value (ρ_{back} and ρ_{tar}), respectively. However, all meshes in TempGroup can have different resistivity vaules ($\rho_{temp,i}$, $i = 1,\cdots,n-2$).

The SPSA reconstruction algorithm for EIT can be formulated as follows. We will iteratively reconstruct an image that fits best the measured voltages U_l at the l th electrode. To do so, we will calculate at each iteration the pseudo voltages $V_l(\rho)$ that correspond to the present state of the reconstructed image. We assume that, by minimizing the difference between the measured voltages and the pseudo voltages, the reconstructed image will converge towards the sought-after original image. Therefore we choose as cost function a following function of the relative difference between the computed and measured potentials on the object boundary

$$E(\rho) = \frac{1}{M}\sum_{i=1}^{M}\left(\frac{U_i - V_i(\rho)}{U_i}\right)^2 \tag{8}$$

The step-by-step summary below shows how SPSA iteratively produces a sequence of estimates [16].

Step 1 Initialization and coefficient selection.

Set counter index $k = 0$. Pick initial guess $\hat{\theta}$ and nonnegative coefficients a, c, A, α, and γ in the SPSA gain sequences $a_k = a/(A+k+1)^\alpha$ and $c_k = c/(k+1)^\gamma$. Practically effective (and theoretically valid) values for α and γ are 0.602 and 0.101, respectively (the asymptotically optimal values of 1.0 and 1/6 may also be used).

Step 2 Generation of simultaneous perturbation vector.

Generate by Monte Carlo a p-dimensional random perturbation vector Δ_k, where each of the p components of Δ_k are independently generated from a zero-mean probability distribution satisfying the conditions in Spall [6]. A simple (and theoretically valid) choice for each component of Δ_k is to use a Bernoulli ± 1 distribution with probability of 0.5 for each ± 1 outcome.

Step 3 Cost function evaluations.

Obtain two measurements of the cost function $E(\ )$ based on

the simultaneous perturbation around the current $\hat{\theta}_k$: $y(\hat{\theta}_k + c_k\Delta_k)$ and $y(\hat{\theta}_k - c_k\Delta_k)$ with the c_k and Δ_k from Step 1 and 2.

Step 4 Gradient approximation.

Generate the simultaneous perturbation approximation to the unknown gradient $g(\hat{\theta}_k)$:

$$\hat{g}_k(\hat{\theta}_k) = \frac{y(\hat{\theta}_k + c_k\Delta_k) - y(\hat{\theta}_k - c_k\Delta_k)}{2c_k} \begin{bmatrix} \Delta_{k1}^{-1} \\ \Delta_{k2}^{-1} \\ \bullet \\ \Delta_{kp}^{-1} \end{bmatrix}$$

Where Δ_{ki} is the i th component of the Δ_k vector (which may be ± 1 random variables as discussed in Step 2). Note that the common numerator in all p components of $\hat{g}_k(\hat{\theta}_k)$ reflects the simultaneous perturbation of all components in $\hat{\theta}_k$ in contrast to the component-by-component perturbations in the standard finite-difference approximation.

Step 5 Updating θ estimate.

Use the standard stochastic approximation from

$$\hat{\theta}_{k+1} = \hat{\theta}_k - a_k \hat{g}_k(\hat{\theta}_k)$$

To update $\hat{\theta}_k$ to a new value $\hat{\theta}_{k+1}$.

Step 6 Iteration or termination.

Return to Step 2 with $k+1$ replacing k . Terminate the algorithm if there is little change in several successive iterates or the maximum allowable number of iterations has been reached.

The choice of the gain sequences (a_k and c_k) is critical to the performance of SPSA. With α and γ as specified in Step 1, one typically finds that in a high-noise setting it is necessary to pick a smaller a and larger c than in a low-noise setting. Although the asymptotically optimal values of α and γ are 1.0 and $1/6$, respectively, it appears that choosing $\alpha < 1.0$ usually yields better finite-sample performance through maintaining a larger step size; hence the recommendation in Step 1 to use values (0.602 and 0.101) that are effectively the lowest allowable satisfying the theoretical conditions mentioned [6]. In a setting where a large amount of data are likely to be available, it may be beneficial to convert to $\alpha = 1.0$ and $\gamma = 1/6$ at some point in the iteration process to take advantage of their asymptotic optimality

3. COMUTER SIMULATION

The proposed algorithm has been tested by comparing its results for numerical simulations with those obtained by mNR method. For the current injection the trigonometric current patterns were used. For the forward calculations, the domain Ω was a unit disc and the mesh of 3104 triangular elements (M=3104) with 1681 nodes (N=1681) and 32 channels (L=32) was used as shown in Figure 1(a). A different mesh system with 776 elements (M=776) and 453 nodes (N=453) was adopted for the inverse calculations as shown in Figure 1(b). In this paper, under the assumption that the resistivity varies only in the radial direction within a cylindrical coordinate system [16], the results of the two inverse problem methods can be easily compared. The resistivity profile given to the finite element inverse solver varies from the center to the boundary of object and is divided into 9 radial elements ($\rho_1, \cdots, \rho_9$) in Figure 1(b).

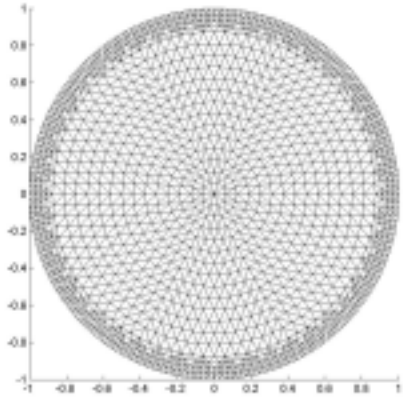

(a)

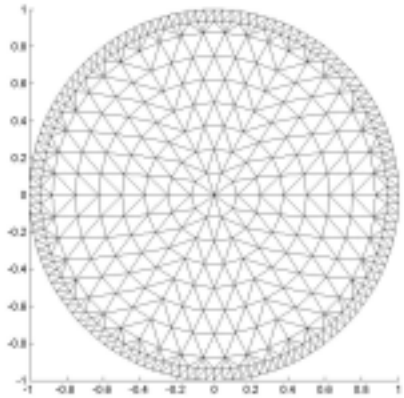

(b)

Fig. 1 Finite element mesh used in the calculation. (The resistivities of the elements within an annular ring are identical.) (a) mesh for forward solver, (b) mesh for inverse solver

The resolution of the method is determined by a number of variables including restivity contrast and distribution, position within the domain, and even current patterns. The ability to positively distinguish between two similar resistivity distributions also depends upon the precision of the voltage measurements. These factors necessitate caution when designing an experiment and interpreting results. Therefore, to verify the appropriateness of EIT for this application, a computational experiment was conducted.

Synthetic boundary potentials were computed for idealized

resistivity distributions using the finite element method described earlier. The boundary potentials were then used for inversion and the results were compared to the original resistivity profiles. The resistivity profile appearing in Figure 2 contains two large discontinuities in the original resistivity distribution. The present example is a severe test in EIT problems because there are large step changes at r/R =0.56 and 0.81 preventing electric currents from going into the center region.

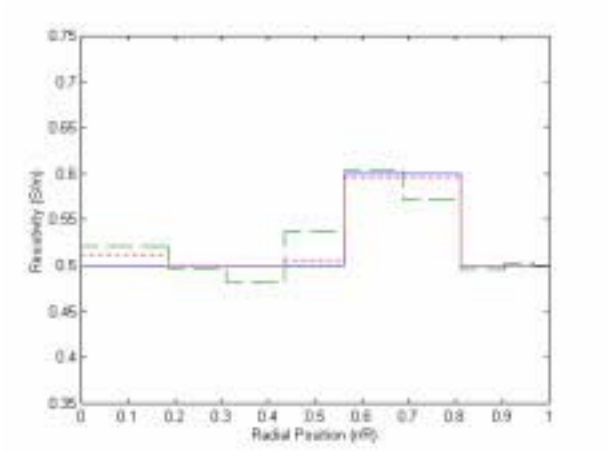

Fig. 2 True resistivities (solid line) and computed resistivities using mNR (dashed line) and SPSA (dotted line).

We started the mNR iteration without any mesh grouping with a homogeneous initial guess. In Table 1, we see that the mNR algorithm may roughly estimate the given true resistivities. Since the mNR have a large error at the boundary of target and background in Figure 2, we can not obtain reconstructed images of high spatial resolution. This kind of poor convergence is a very typical problem in the NR-type algorithms.

Table 1 The caption should be placed before the table.

	ρ_1	ρ_2	ρ_3	ρ_4	ρ_5	ρ_6	ρ_7	ρ_8	ρ_9
Real	0.5	0.5	0.5	0.5	0.6	0.6	0.5	0.5	0.5
mNR	.521	.497	.483	.538	.603	.572	.496	.502	.499
SPSA	.511	.500	.500	.506	.596	.596	.500	.500	.500

However, we can significantly improve the mNR's poor convergence by adopting the proposed SPSA via a two-step approach as follows. In the first step, we adopted a mNR method as a basic image reconstruction algorithm. After a few initial mNR iterations performed without any grouping, we rearrange the resisitivity values of meshes by sorting them in ascending order. Then the boundary location between regions can be roughly decided and mesh be determined to the target, background, or undetermined temporary group. In this paper, from the Table 1, 2 meshes (ρ_5, ρ_6) and 5 meshes ($\rho_2, \rho_3, \rho_7, \rho_8, \rho_9$) among 9 may be grouped to TargetGroup (ρ_{tar}) and BackGroup (ρ_{back}), respectively. The remainders of meshes (ρ_1, ρ_4) are grouped to TempGroup. Hence, the number of unknowns is reduced to 4.

In the second step, after mesh grouping, we will determine the values of these resistivities using SPSA algorithm. The SPSA solves the EIT problem, searching for the resistivities ($\rho_1, \rho_4, \rho_{tar}$ and ρ_{back}) minimizing the reconstruction error. In this case, we will use ρ_{back} (or ρ_{tar}) as the minimum (or maximum) values of the unknown resistivity distribution. The computed resistivities in SPSA are constrained between the minimum and maximum values. The initial values of unknown ρ_{tar} and ρ_{back} are the average resistivity values of meshes in BackGroup and TargetGroup, respectively. From Figure 2 and Table 1, the inverted profile using SPSA matches the original profile very well near the wall at r/R =1.0 as well as the center at r/R =0.0. Furthermore, the SPSA reconstruction is successful for the jump of resistivty at r/R =0.56 and 0.81.

4. CONCLUSION

In this paper, an EIT image reconstruction method based on SPSA via two-step approach was presented to improve the spatial resolution. A technique based on SPSA algorithm with the knowledge of mNR was developed for the solution of the EIT inverse problem. Although SPSA is expensive in terms of computing time and resources, which is a weakness of the method that renders it presently unsuitable for real-time tomographic applications, the exploitation of a priori knowledge will produce very good reconstructions. Further extensions include an EIT image reconstruction to multi-resistivity value problems.

ACKNOWLEDGMENTS

This work was supported by the Nuclear Academic Research Program by the Ministry of Science and Technology (MOST).

REFERENCES

[1] J. G. Webster, Electrical Impedance Tomography, Adam Hilger, 1990.

[2] J. C. Newell, D. G. Gisser, and D. Isaacson, "An electric current tomograph," IEEE Trans. on Biomedical Engineering, vol. 35, no. 10, pp. 828-833, 1987.

[3] M. Vauhkonen, Electrical Impedance Tomography and Priori Information, Kuopio Univerisity Publications Co., Natural and Environmental Sciences 62, 1997.

[4] T. J. Yorkey, J. G. Webster, and W. J. Tompkins, "Comparing reconstruction algorithms for electrical impedance tomography," IEEE Trans. on Biomedical Engineering, vol. 34, no. 11, pp. 843-852, 1987.

[5] J. C. Spall, "A stochastic approximation technique for generating maximum likelihood parameter estimates," American Control Conference, pp. 1161-1167, 1987.

[6] J. C. Spall, "Multivariate stochastic approximation using a simultaneous perturbation gradient approximation," IEEE Trans. on Automatic Control, vol. 37, pp. 332-341, 1992.

[7] J. E. Dennis and R. B. Schnabel, "A view of unconstrained optimization," Optimization, Handbooks

in OR & MS, vol. 1, ch. 1, pp. 1-72, 1989.
[8] M. Glidewell and K. T. Ng, “Anatomically constrained electrical impedance tomography for anisotropic bodies via a two-step approach,” IEEE Trans. on Medical Imaging, vol. 14, no. 3, pp. 498-503, 1995.
[9] K. D. Paulsen, P. M. Meaney, M. J. Moskowitz, and J.M. Sullivan, “A dual mesh scheme for finite element based reconstruction algorithm,” IEEE Trans. on Medical Imaging, vol. 14, no. 3, pp. 504–514, 1995.
[10] T. Murai and Y. Kagawa, “Electrical impedance computed tomography based on a finite element model,” IEEE Trans. on Biomedical Engineering, vol. 32, no. 3, pp. 177-184, 1985.
[11] C. Cohen-Bacrie, Y. Goussard, and R. Guardo, “Regularized reconstruction in electrical impedance tomography using a variance uniformization constraint,” IEEE Trans. on Medical Imaging, vol. 16, no. 5, pp. 170-179, 1997.
[12] M. Vauhkonen, D. Vadasz, P. A. Karjalainen, and J. P. Kaipio, “Subspace regularization method for electrical impedance tomography,” 1st International Conference on Bioelectromagnetism, Tampere, Finland, pp. 9-13, 1996.
[13] A. Adler and R. Guardo, “Electrical impedance tomography: regularized imaging and contrast detection,” IEEE Trans. on Medical Imaging, vol. 15, no. 2, pp. 170-179, 1996.
[14] C. J. Grootveld, A. Segal, and B. Scarlett, “Regularized modified Newton-Raphson technique applied to electrical impedance tomography,” International Journal of Imaging System Technology, vol. 9, pp. 60-65, 1998.
[15] M. C. Kim, S. Kim, K. Y. Kim, J. H. Lee, and Y. J. Lee, “Reconstruction of particle concentration distribution in annular Couette flow using electrical impedance tomography,” J. Ind. Eng. Chem., vol. 7, no. 5, pp. 341-347, 2001.
[16] J. C. Spall, “Implementation of the simultaneous perturbation algorithm for stochastic optimization,” IEEE Trans. on Aerospace and Electronic Systems, vol. 34, no. 3, pp. 817-823, 1998.